



Sylvestre, M. A. S., Teanby, N. A., Dobrijevic, M., Sharkey, J., & Irwin, P. G. J. (2020). C<sub>2</sub>N<sub>2</sub> vertical profile in Titan's stratosphere. *Astronomical Journal*, 160(4), [178]. <https://doi.org/10.3847/1538-3881/abafb2>

Peer reviewed version

Link to published version (if available):  
[10.3847/1538-3881/abafb2](https://doi.org/10.3847/1538-3881/abafb2)

[Link to publication record in Explore Bristol Research](#)  
PDF-document

This is the author accepted manuscript (AAM). The final published version (version of record) is available online via IOP Publishing at <https://doi.org/10.3847/1538-3881/abafb2>. Please refer to any applicable terms of use of the publisher.

## University of Bristol - Explore Bristol Research

### General rights

This document is made available in accordance with publisher policies. Please cite only the published version using the reference above. Full terms of use are available: <http://www.bristol.ac.uk/red/research-policy/pure/user-guides/ebr-terms/>

## C<sub>2</sub>N<sub>2</sub> vertical profile in Titan's stratosphere

2 M. SYLVESTRE,<sup>1</sup> N. A. TEANBY,<sup>1</sup> M. DOBRIJEVIC,<sup>2</sup> J. SHARKEY,<sup>1</sup> AND P. G. J. IRWIN<sup>3</sup>

3 <sup>1</sup>*School of Earth Sciences, University of Bristol, Wills Memorial Building, Queens Road, Bristol BS8 1 RJ, UK*

4 <sup>2</sup>*Laboratoire d'astrophysique de Bordeaux, Univ. Bordeaux, CNRS, B18N, allée Geoffroy Saint-Hilaire, 33615 Pessac,*  
5 *France*

6 <sup>3</sup>*Atmospheric, Oceanic, & Planetary Physics, Department of Physics, University of Oxford, Clarendon Laboratory,*  
7 *Parks Road, Oxford OX1 3PU, UK*

8 Submitted to Astronomical Journal

### 9 ABSTRACT

10 In this paper, we present the first measurements of the vertical distribution of  
11 cyanogen (C<sub>2</sub>N<sub>2</sub>) in Titan's lower atmosphere at different latitudes and seasons, us-  
12 ing Cassini/CIRS far-IR data. We also study the vertical distribution of three other  
13 minor species detected in our data: methylacetylene (C<sub>3</sub>H<sub>4</sub>), diacetylene (C<sub>4</sub>H<sub>2</sub>) and  
14 H<sub>2</sub>O, in order to compare them to C<sub>2</sub>N<sub>2</sub>, but also to get an overview of their seasonal  
15 and meridional variations in Titan's lower stratosphere from 85 km to 225 km. We  
16 measured an average volume mixing ratio of C<sub>2</sub>N<sub>2</sub> of  $6.2 \pm 0.8 \times 10^{-11}$  at 125 km at  
17 the equator, but poles exhibit a strong enrichment in C<sub>2</sub>N<sub>2</sub> (up to a factor 100 com-  
18 pared to the equator), greater than what was measured for C<sub>3</sub>H<sub>4</sub> or C<sub>4</sub>H<sub>2</sub>. Measuring  
19 C<sub>2</sub>N<sub>2</sub> profiles provides constraints on the processes controlling its distribution, such  
20 as bombardment by Galactic Cosmic Rays which seem to have a smaller influence on  
21 C<sub>2</sub>N<sub>2</sub> than predicted by photochemical models.

### 22 1. INTRODUCTION

23 Titan's atmosphere is mainly composed of N<sub>2</sub>  
24 (98%) and CH<sub>4</sub> (between 1% and 1.5% in the  
25 stratosphere, in [Lellouch et al. 2014](#); [Bézard  
26 2014](#); [Niemann et al. 2010](#)), but also hosts a  
27 large variety of trace gases. Hydrocarbons and  
28 nitriles (C<sub>x</sub>H<sub>y</sub>N<sub>z</sub>) such as C<sub>2</sub>H<sub>2</sub> and HCN are  
29 produced by the dissociation of the two main  
30 atmospheric components by solar UV and EUV  
31 photons, Saturn's magnetospheric electrons and  
32 Galactic Cosmic Rays (GCR), and by the sub-  
33 sequent reactions between the different species

Corresponding author: M. Sylvestre  
[melody.sylvestre@bristol.ac.uk](mailto:melody.sylvestre@bristol.ac.uk)

34 produced ([Vuitton et al. 2019](#)). The oxygen  
35 bearing species CO, CO<sub>2</sub> and H<sub>2</sub>O were also  
36 detected (e.g [Lutz et al. 1983](#); [Samuelson et al.  
37 1983](#); [Coustenis et al. 1998](#)) although the origin  
38 of the oxygen is not fully understood. Different  
39 sources such as Enceladean plumes or microm-  
40 eteorite ablation have been proposed (e.g in  
41 [Hörst et al. 2008](#); [Dobrijevic et al. 2014](#)). Char-  
42 acterizing the spatial distribution of Titan's  
43 trace gases and their temporal variations allow  
44 us to better understand the chemical and dy-  
45 namical processes of its atmosphere and how  
46 they are affected by the seasonal variations of  
47 insolation caused by Titan's obliquity (26.7°).  
48 The data from the Cassini mission have been  
49 particularly helpful as they provided a monitor-

ing of Titan’s atmosphere from 2004 to 2017,  
i.e. from northern winter to summer solstice  
(Nixon et al. 2019).

In this paper, we focus on  $C_2N_2$  (cyanogen)  
as its distribution in Titan’s atmosphere is not  
very well constrained. Cui et al. (2009) used  
Cassini/INMS data and measured an abun-  
dance of  $C_2N_2$  of  $4.8 \pm 0.8 \times 10^{-5}$  in the ther-  
mosphere (1077 km). In the stratosphere, the  
meridional distribution of  $C_2N_2$  and its seasonal  
evolution around 85 km have been studied with  
Cassini/CIRS (Sylvestre et al. 2018; Teanby  
et al. 2009) and previously with Voyager I/IRIS  
(Coustenis & Bezdard 1995). However, the verti-  
cal distribution of  $C_2N_2$  has only been measured  
once at  $70^\circ N$  in 1980 (during northern spring),  
by Coustenis et al. (1991) using Voyager I/IRIS.  
This polar profile is not directly comparable  
with photochemical models, which typically use  
low latitudes or equatorial conditions.

In the present study, we measured  $C_2N_2$  ver-  
tical profiles in Titan’s stratosphere, using  
Cassini/CIRS data to cover different latitudes  
and seasons. We compared the  $C_2N_2$  verti-  
cal distribution and its seasonal evolution with  
other species present in our data such as  $C_3H_4$ ,  
 $C_4H_2$  and  $H_2O$  to better understand the atmo-  
spheric processes at play in Titan’s atmosphere.

## 2. DATA ANALYSIS

### 2.1. Observations

We used observations from the thermal in-  
frared spectrometer Cassini/CIRS (Composite  
InfraRed Spectrometer, Flasar et al. 2004; Jen-  
nings et al. 2017; Nixon et al. 2019). CIRS  
is composed of three focal planes operating  
at different wavenumbers:  $10 - 600 \text{ cm}^{-1}$   
( $17 - 1000 \text{ }\mu\text{m}$ ) for FP1,  $600 - 1100 \text{ cm}^{-1}$   
( $9 - 17 \text{ }\mu\text{m}$ ) for FP3, and  $1100 - 1400 \text{ cm}^{-1}$   
( $7 - 9 \text{ }\mu\text{m}$ ) for FP4.

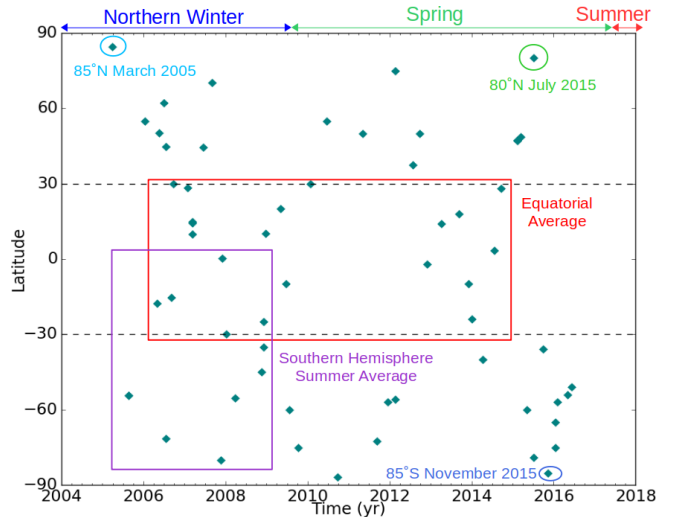


**Figure 1.** Spatial and temporal distribution of the limb datasets presented in this paper. Teal diamonds represent the available Cassini/CIRS limb data. Spatial averages indicated with rectangles.

In this study, we analysed limb (line of sight  
perpendicular to the local vertical) and nadir  
(line of sight toward the centre of Titan) FP1  
spectra in the  $200 - 350 \text{ cm}^{-1}$  range, with a  
spectral resolution of  $0.5 \text{ cm}^{-1}$  and a sampling  
interval of  $0.25 \text{ cm}^{-1}$ . During the limb observa-  
tions, spectra are measured at 125 km and 225  
km of altitude. The response of the FP1 de-  
tector can be represented by a Gaussian with a  
50% integrated response diameter of 2.54 mrad,  
truncated at a radius  $r = 1.95 \text{ mrad}$  from the  
centre of the field of view (Teanby & Irwin  
2007; Flasar et al. 2004), which corresponds to  
a vertical field of view of 70 km on average. For  
each altitude, an acquisition lasts from 10 to  
30 minutes, which allows recording of 7 to 45  
spectra, which are averaged together to increase  
the S/N by a factor  $\sqrt{N}$  (with  $N$  the number  
of spectra). Nadir observations are realised in  
”sit-and-stare” geometry where the detector  
probes the same latitude and longitude during  
the acquisition, with an average field of view  
of  $20^\circ$  of latitude. For each observation, 100  
to 330 spectra were acquired over a 1.5 - 4.5  
hour period. These spectra were then averaged

117 together.

118

119 Figure 1 shows the spatial and temporal dis-  
 120 tribution of all the available FP1 limb obser-  
 121 vations with a spectral resolution of  $0.5 \text{ cm}^{-1}$ .  
 122 In most datasets (datasets not acquired pole-  
 123 ward from  $60^\circ\text{S}$  in autumn winter, or poleward  
 124 from  $60^\circ\text{N}$  at all seasons), the  $\text{C}_2\text{N}_2$  band at  
 125  $234 \text{ cm}^{-1}$  (see fig. 2) was too weak to enable  
 126 the retrieval of the molecule’s vertical profile.  
 127 That is why we chose to focus on a few spe-  
 128 cific datasets, representative of different seasons  
 129 and latitudes and grouped other more equato-  
 130 rial datasets together to improve the signal to  
 131 noise. We measured the vertical distribution of  
 132  $\text{C}_2\text{N}_2$  at  $85^\circ\text{N}$  in 2005 (during northern winter),  
 133 at  $80^\circ\text{N}$  in 2015 (during northern spring), at  
 134  $85^\circ\text{S}$  in 2015 (during southern autumn), and  
 135 we averaged all the spectra measured in the  
 136 southern hemisphere between 2005 and 2009  
 137 during southern summer, and in the equatorial  
 138 area ( $30^\circ\text{N}$ - $30^\circ\text{S}$ ) over the duration of the mis-  
 139 sion. These averages will be later respectively  
 140 designated as ”southern hemisphere summer  
 141 average” and ”equatorial average”. For each  
 142 of them, a preliminary inspection of the in-  
 143 cluded datasets showed weak variations of radi-  
 144 ances in the  $\text{C}_2\text{N}_2$  band for similar temperatures  
 145 (e.g Mathé et al. 2019; Sylvestre et al. 2019).  
 146 **This suggested that strong variations of**  
 147  **$\text{C}_2\text{N}_2$  were not present within these av-**  
 148 **erages.** Effects of the averages on retrieved  
 149 abundances were assessed by comparing our  
 150 results for  $\text{C}_4\text{H}_2$  and  $\text{C}_3\text{H}_4$  with previous non-  
 151 averaged CIRS observations at similar times  
 152 and latitudes (see Section 3.1). For each case,  
 153 we associate limb and nadir spectra measured  
 154 at similar epoch (within a year) and latitude  
 155 (within  $5^\circ$ ), to obtain measurements at three  
 156 different altitudes (225 km and 125 km with the  
 157 limb observations, 85 km with the nadir obser-  
 158 vations) and probe Titan’s lower stratosphere.  
 159 The datasets presented in this study are listed

160 in Tables 1 and 2.

161

162

## 2.2. Retrieval method

163 Figure 2 shows examples of limb spectra in the  
 164  $200 - 350 \text{ cm}^{-1}$  range. We measure the abun-  
 165 dance of  $\text{C}_2\text{N}_2$  using its  $\nu_5$  band at  $234 \text{ cm}^{-1}$ .  
 166 Other spectral features are visible such as the  $\nu_9$   
 167 band of  $\text{C}_4\text{H}_2$  at  $220 \text{ cm}^{-1}$ ,  $\nu_{10}$  band of  $\text{C}_3\text{H}_4$  at  
 168  $327 \text{ cm}^{-1}$ , and several absorption bands of  $\text{H}_2\text{O}$ ,  
 169 for instance at  $202 \text{ cm}^{-1}$ ,  $208 \text{ cm}^{-1}$ ,  $228 \text{ cm}^{-1}$ ,  
 170 and  $254 \text{ cm}^{-1}$ . We retrieve the abundances  
 171 of these gases using the constrained non-linear  
 172 inversion code NEMESIS (Irwin et al. 2008).  
 173 NEMESIS uses an iterative algorithm where  
 174 a synthetic spectrum is calculated from a ref-  
 175 erence atmosphere and *a priori* values for the  
 176 retrieved parameters. For each iteration, these  
 177 values are updated to minimise the difference  
 178 between the measured and the synthetic spec-  
 179 tra, until convergence is reached and the im-  
 180 provement in misfit is less than 0.1%.

181

182 We adopt the same reference atmosphere  
 183 as Sylvestre et al. (2018) which takes into  
 184 account the abundances of the main con-  
 185 stituents of Titan’s atmosphere, as measured  
 186 by Cassini/CIRS, Cassini/VIMS, ALMA , and  
 187 Huygens/GCMS. The composition of this ref-  
 188 erence atmosphere and the relevant references  
 189 are fully detailed in Sylvestre et al. (2018).

190

191 Aerosol properties and vertical distributions  
 192 are derived from previous Cassini/CIRS mea-  
 193 surements of de Kok et al. (2007, 2010); Vinatier  
 194 et al. (2012), with the four types of hazes de-  
 195 scribed in de Kok et al. (2007): hazes 0 ( $70 \text{ cm}^{-1}$   
 196 to  $400 \text{ cm}^{-1}$ ), A (centred at  $140 \text{ cm}^{-1}$ ), B (cen-  
 197 tred at  $220 \text{ cm}^{-1}$ ) and C (centred at  $190 \text{ cm}^{-1}$ ).

198

199 Spectroscopic parameters are the same as in  
 200 Sylvestre et al. (2018), except for the Col-  
 201 lision Induced Absorption coefficients (CIA).  
 202 We adopted the model presented in Bézard

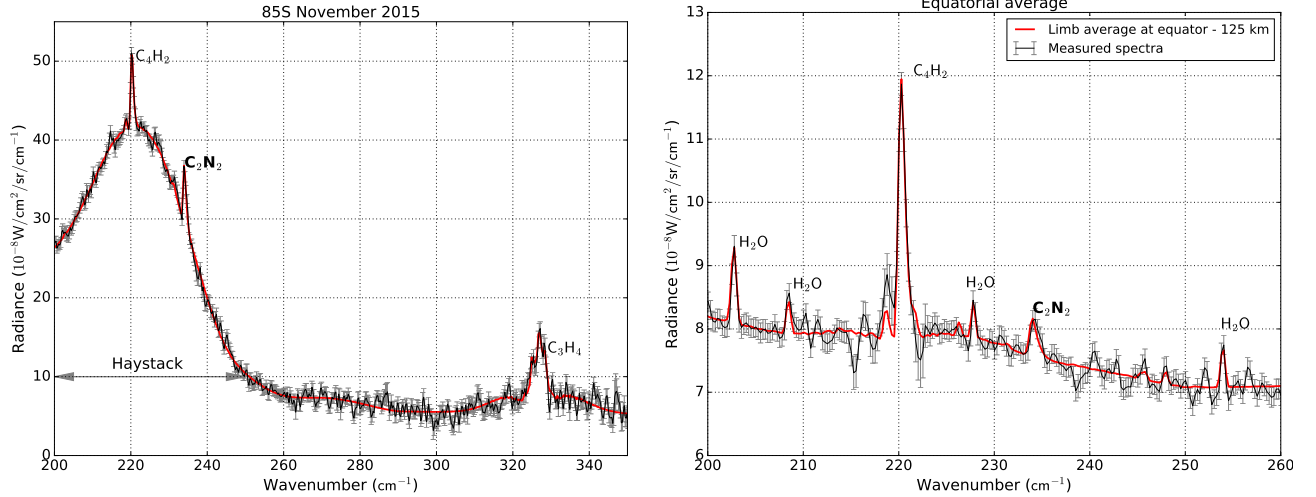


**Figure 2.** Examples of spectra measured with Cassini/CIRS (black lines) and matching synthetic spectra calculated by NEMESIS (red lines). The spectral resolution is  $0.5 \text{ cm}^{-1}$ ; data points are spaced by  $0.25 \text{ cm}^{-1}$ . *Left panel:* Limb spectrum measured at  $85^\circ\text{S}$  in November 2015 at 125 km. Note the presence of the haystack feature, which is visible only in limb and nadir far-IR spectra measured at high latitudes (poleward from  $60^\circ$ ) in autumn and winter.  $\text{H}_2\text{O}$  bands are not visible at high latitudes. *Right panel:* Average of all the limb spectra measured at 125 km between  $30^\circ\text{N}$  and  $30^\circ\text{S}$  over the duration of the Cassini mission (later referenced as "equatorial average"), with a close-up on the  $200\text{--}260 \text{ cm}^{-1}$  region where  $\text{C}_2\text{N}_2$ ,  $\text{C}_4\text{H}_2$  and  $\text{H}_2\text{O}$  bands are visible.

203 & Vinatier (2019), where the coefficients for  
 204 the  $\text{N}_2 - \text{CH}_4$  CIA from Borysow & Tang  
 205 (1993) and the  $\text{N}_2 - \text{N}_2$  CIA from Borysow &  
 206 Frommhold (1986a) are multiplied by the fol-  
 207 lowing factors:

$$C_{\text{N}_2-\text{CH}_4} = 1 + \frac{0.5}{(T - T_{\text{sat}})^2 + 1} \quad (1)$$

$$C_{\text{N}_2-\text{N}_2} = 2^{\frac{\sigma-110}{2.5 \times T-100}} \quad (2)$$

208 where  $T$ ,  $T_{\text{sat}}$  and  $\sigma$  are respectively local  
 209 temperature,  $\text{CH}_4$  saturation temperature and  
 210 wavenumber. Coefficients for  $\text{H}_2 - \text{N}_2$  and  
 211  $\text{CH}_4 - \text{CH}_4$  CIA remain the same as in Borysow  
 212 & Frommhold (1986b, 1987).

213 For each of the cases presented in figure 1,  
 214 limb and nadir spectra were fitted individually  
 215 as follow:

216 *Southern summer hemisphere average and  $80^\circ\text{N}$*   
 217 *in July 2015*—For each limb spectrum, we re-  
 218 trieved scale factors toward the nominal pro-  
 219 files of  $\text{C}_2\text{N}_2$ ,  $\text{C}_3\text{H}_4$ ,  $\text{C}_4\text{H}_2$ ,  $\text{H}_2\text{O}$ , and the four  
 220 types of hazes previously defined. The effect of

221 the large field of view of the CIRS FP1 limb  
 222 data was taken into account by dividing their  
 223 field of view into  $M$  parts, generating synthetic  
 224 spectra for each of these parts, and using a  
 225 weighted average of these spectra, as described  
 226 in Teanby & Irwin (2007). We chose  $M = 11$   
 227 so that the errors in the modelled radiance stay  
 228 smaller than the measurement noise. We set the  
 229 temperature profiles for the considered latitudes  
 230 and dates using previous Cassini/CIRS mea-  
 231 surements of Sylvestre et al. (2019) and Teanby  
 232 et al. (2019). For each gas, we used the abun-  
 233 dances retrieved from the two limb spectra (at  
 234 125 km and 225 km) to build *a priori* profiles for  
 235 the nadir retrievals. We then retrieved  $\text{C}_2\text{N}_2$ ,  
 236  $\text{C}_3\text{H}_4$ ,  $\text{C}_4\text{H}_2$ , and  $\text{H}_2\text{O}$  scale factors from the  
 237 nadir spectra using these *a priori* profiles. We  
 238 also retrieved simultaneously scale factors for  
 239 hazes 0, B, and C and a temperature profile (as  
 240 the tropospheric temperature contributes to the  
 241 continuum emission of the nadir spectra).



242 85°N in March 2005 and 85°S in November 2015  
 243 —The previous method had to be adapted to  
 244 these datasets, in order to fit the haystack fea-  
 245 ture (see fig. 2) in both limb and nadir spectra.  
 246 We retrieved the cross-sections of haze B for  
 247 each spectrum while keeping the vertical distri-  
 248 bution measured in de Kok et al. (2007). We  
 249 also retrieve simultaneously scale factors for  
 250 C<sub>2</sub>N<sub>2</sub>, C<sub>3</sub>H<sub>4</sub>, C<sub>4</sub>H<sub>2</sub>, H<sub>2</sub>O and haze 0 profiles,  
 251 and a temperature profile (only for the nadir  
 252 spectra).

254 *Equatorial average*—We follow a method similar  
 255 as in the first case, except that this time, it was  
 256 necessary to fit new cross-sections for haze 0 in  
 257 each limb spectrum while scale factors were re-  
 258 trieved for hazes B and C. This difference could  
 259 be due to the fact that the equatorial average  
 260 was made by averaging CIRS spectra over 8  
 261 years, unlike the other datasets where spectra  
 262 were measured at a single date or over a half a  
 263 season (2005-2009 for the southern hemisphere  
 264 summer average).

266 Errors due to measurement noise, forward  
 267 modelling and smoothing of the profiles by  
 268 NEMESIS and are on the order of 10% on av-  
 269 erage. For the equatorial average, as we used  
 270 an average temperature profile as *a priori*, we  
 271 assess the effects of temperature variations on  
 272 the considered latitude and time range by re-  
 273 trieving these datasets using the coldest and  
 274 warmest temperature profiles measured at the  
 275 equator over the Cassini mission. We found  
 276 that the errors due to temperature variations  
 277 are also about 10%.

279 For each dataset, the level of detection of a  
 280 gas can be assessed by calculating the change  
 281 in the misfit  $\Delta\chi^2$ , defined as:

$$\Delta\chi^2 = \chi^2 - \chi_0^2 \quad (3)$$

282 with:

$$\chi^2 = \sum_{i=1}^N \frac{(I_{mes}(w_i) - I_{fit}(w_i, x))^2}{2\sigma_i^2} \quad (4)$$

283 where  $I_{mes}$  and  $I_{fit}$  are respectively the mea-  
 284 sured and fitted radiance, at a given wavenum-  
 285 ber  $w_i$  and for a value  $x$  of the abundance of  
 286 the considered gas.  $\sigma_i$  is the measurement er-  
 287 ror at  $w_i$ . The factor 2 at the denominator is  
 288 to calculate the  $\chi^2$  for the correct number of  
 289 independent points, as spectra have a sampling  
 290 interval of 0.25 cm<sup>-1</sup> while their spectral reso-  
 291 lution is 0.5 cm<sup>-1</sup>.  $\chi_0^2$  is the value of  $\chi^2$  with  
 292  $x = 0$ . In the datasets presented here, C<sub>4</sub>H<sub>2</sub> and  
 293 C<sub>3</sub>H<sub>4</sub> were always detected at more than 3- $\sigma$   
 294 ( $\Delta\chi^2 \leq -9$ ). When C<sub>2</sub>N<sub>2</sub> and H<sub>2</sub>O were not  
 295 detected at 3  $\sigma$ , we looked for their 3- $\sigma$  upper  
 296 limits, i.e. the value  $x$  for which  $\Delta\chi^2 = 9$ .  
 297 This was especially relevant at the poles, where  
 298 water could not be detected at more than 1- $\sigma$ ,  
 299 and for C<sub>2</sub>N<sub>2</sub> which could not be detected at  
 300 the equator at 225 km.

302 Figure 3 shows the normalized contribution  
 303 functions for C<sub>4</sub>H<sub>2</sub> (at 220.25 cm<sup>-1</sup>), C<sub>2</sub>N<sub>2</sub> (at  
 304 234 cm<sup>-1</sup>), C<sub>3</sub>H<sub>4</sub> (at 326.75 cm<sup>-1</sup>), and H<sub>2</sub>O (at  
 305 202 cm<sup>-1</sup>). Taking into account their field of  
 306 view, the combination of limb and nadir data  
 307 are sensitive in the 75-265 km altitude range for  
 308 C<sub>2</sub>N<sub>2</sub>, C<sub>4</sub>H<sub>2</sub> and C<sub>3</sub>H<sub>4</sub>, and in the 90-265 km  
 309 range for H<sub>2</sub>O. C<sub>2</sub>N<sub>2</sub> and C<sub>3</sub>H<sub>4</sub> contribution  
 310 functions are similar for the equatorial aver-  
 311 age and 85°S in 2015. However, the cold polar  
 312 temperatures of southern autumn increase the  
 313 altitude at which C<sub>4</sub>H<sub>2</sub> condenses, shift the  
 314 contribution function of the nadir spectra up-  
 315 wards (from 85 km to 95 km), and make the  
 316 contribution function of the limb spectrum at  
 317 125 km narrower.

### 319 3. RESULTS AND DISCUSSIONS

#### 320 3.1. C<sub>3</sub>H<sub>4</sub> and C<sub>4</sub>H<sub>2</sub>

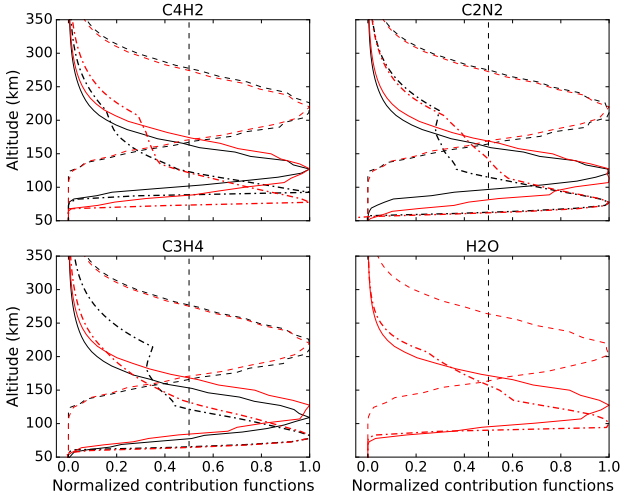


**Figure 3.** Normalized contribution functions for the equatorial average (in red) and 85°S in November 2015 (in black). Solid and dashed lines represent respectively the contribution functions for the limb data at 125 km and 225 km. Dot-dashed lines stand for nadir data. The combination of the limb and nadir FP1 data allows to measure C<sub>2</sub>N<sub>2</sub>, C<sub>3</sub>H<sub>4</sub>, C<sub>4</sub>H<sub>2</sub> in the 75–265 km range, and H<sub>2</sub>O between 90 km and 245 km. Note that the contribution functions of the equatorial average and for 85°S in November 2015 are often very similar (and hence superimposed), except for the C<sub>4</sub>H<sub>2</sub> nadir and 125 km limb spectra, as the cold polar temperatures shift the C<sub>4</sub>H<sub>2</sub> condensation level upward.

In figure 4 we present the results of our limb and nadir measurements for C<sub>3</sub>H<sub>4</sub>, C<sub>4</sub>H<sub>2</sub>, C<sub>2</sub>N<sub>2</sub>, and H<sub>2</sub>O.

We show our measurements of C<sub>3</sub>H<sub>4</sub> in panel (a) and C<sub>4</sub>H<sub>2</sub> in panel (b). With our equatorial limb and nadir spectral averages over the Cassini mission, we obtained profiles of C<sub>4</sub>H<sub>2</sub> and C<sub>3</sub>H<sub>4</sub> that are increasing with altitude (from  $1.1 \pm 0.05 \times 10^{-9}$  at 85 km to  $4.1 \pm_{0.3}^{0.4} \times 10^{-9}$  at 225 km for C<sub>4</sub>H<sub>2</sub>, and from  $3.7 \pm 0.1 \times 10^{-9}$  at 85 km to  $6.9 \pm_{0.6}^{0.9} \times 10^{-9}$  at 225 km for C<sub>3</sub>H<sub>4</sub>). Previous Cassini/CIRS studies showed that below 300 km, at the equator, trace gases abundances vary weakly throughout the Cassini mission (e.g Mathé et al. 2019;

Teanby et al. 2019). The volume mixing ratios retrieved from our equatorial spectral average should thus be comparable to previous individual measurements at specific times during the Cassini mission. For instance fig. 4 shows that our profiles of C<sub>4</sub>H<sub>2</sub> are in very good agreement with the results of Mathé et al. (2019) with Cassini/CIRS FP3 measurements at 0°N in March 2009, while we measured slightly smaller abundances than them for C<sub>3</sub>H<sub>4</sub>. Lombardo et al. (2019a) averaged Cassini/CIRS FP3 limb spectra acquired between 20°S and 20°N from 2004-2009 and found a nearly constant with altitude volume mixing ratio of  $1 \times 10^{-8}$  between 110 km and 400 km, which is also slightly larger than our results. These differences can be explained by the characteristics of the compared datasets, especially the different vertical coverages and resolutions (10 to 50 km for the limb data of Mathé et al. 2019; Lombardo et al. 2019a), the use of detectors operating in different wavelengths and thus the use of different spectroscopic data. Our results are also consistent with the nadir CIRS FP3 measurements from Coustenis et al. (2019) who measured volume mixing ratios of  $4.9 \pm 1 \times 10^{-9}$  for C<sub>3</sub>H<sub>4</sub> and  $1.1 \pm 0.3 \times 10^{-9}$  for C<sub>4</sub>H<sub>2</sub> at 10 mbar (100 km) at the equator in 2017, and nadir measurements of Teanby et al. (2019) who found average abundances of  $9 \times 10^{-9}$  for C<sub>3</sub>H<sub>4</sub> and  $2 \times 10^{-9}$  at 1 mbar (180 km) at the equator throughout the Cassini mission.

We observe a similar situation when comparing the C<sub>3</sub>H<sub>4</sub> and C<sub>4</sub>H<sub>2</sub> profiles measured from our limb and nadir spectral averages over the southern hemisphere in summer (2005-2009) with: Mathé et al. (2019) at 46°S in December 2007, the measurements of Coustenis et al. (2019) and Teanby et al. (2019), and the average profile of C<sub>3</sub>H<sub>4</sub> in the southern hemisphere measured by Lombardo et al. (2019a) in 2004-2009 (20°S-60°S). Besides, Coustenis

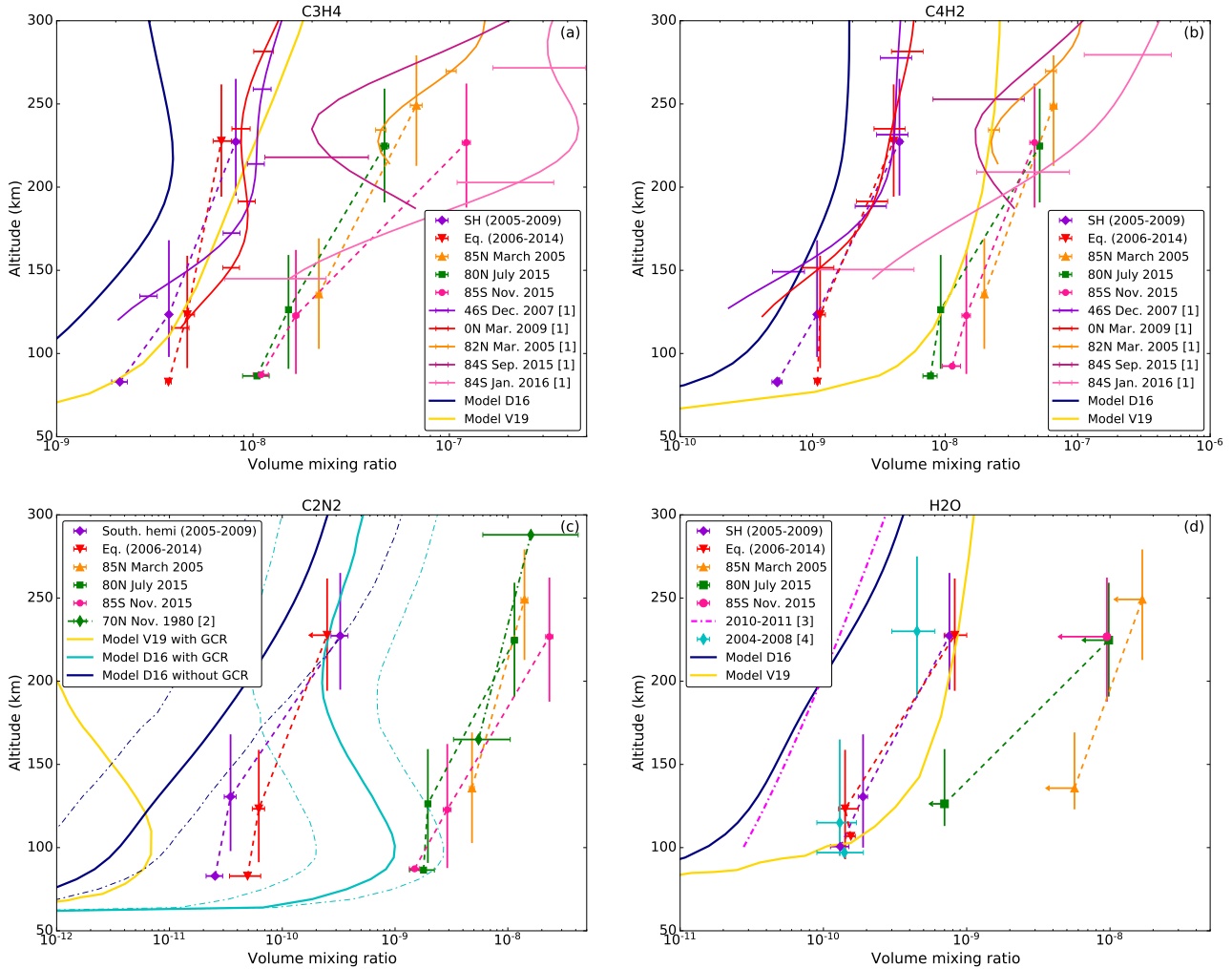


**Figure 4.** Vertical profiles of  $C_3H_4$ ,  $C_4H_2$ ,  $C_2N_2$ , and  $H_2O$ . Markers indicate the volume mixing ratios measured from limb and nadir measurements. Vertical lines represent the field of view of the limb data. Dashed lines help to visualize the vertical variations of these 4 species. V19 and D16 stand respectively for the nominal photochemical model predictions of Vuitton et al. (2019) and Dobrijevic et al. (2016); Loison et al. (2019). Panels (a) and (b): [1] indicates the Cassini/CIRS limb measurements of Mathé et al. (2019). Panels (c) and (d): [2], [3] and [4] are respectively the measurements of Coustenis et al. (1991) with Voyager 1/IRIS, Moreno et al. (2012) with Herschel/PACS and HIFI, and Cottini et al. (2012) with Cassini/CIRS. In panel (c), the uncertainties around the profiles of model D16 are shown for  $C_2N_2$  as thin dot-dashed lines.

380 et al. (2019); Mathé et al. (2019); Teanby et al.  
 381 (2019) showed that trace gas abundances re-  
 382 main fairly constant below 300 km throughout  
 383 southern summer. Consequently our equato-  
 384 rial and summer southern hemisphere averages  
 385 seem to capture fairly well the composition of  
 386 Titan’s atmosphere in the lower atmosphere,  
 387 despite the large latitude and time ranges used.

388 Besides, using nadir FP1 data allows us to  
 389 probe lower altitudes (down to 85 km) than  
 390 the studies cited above, and thus to complete  
 391 them with information about the lower part  
 392 of the stratosphere, as shown in Sylvestre  
 393 et al. (2018); Lombardo et al. (2019b).  
 394 For instance, fig. 4 shows that in summer,  
 395 abundances of  $C_3H_4$  and  $C_4H_2$  in the southern



hemisphere are smaller than at the equator at 85 km (by a factor 2 for  $C_4H_2$ ), while they are similar for both latitudes above 125 km and up to 360 km for  $C_3H_4$  and 440 km for  $C_4H_2$ . When compared to photochemical models predictions, the  $C_3H_4$  profile measured at the equator is in good agreement with the predictions of Vuitton et al. (2019) (model V19 on fig. 4). The model of Dobrijevic et al. (2016); Loison et al. (2019) (model D16 on fig. 4) underestimates the abundance of this gas by up to a factor 10 at 85 km. The abundances predicted by Dobrijevic et al. (2016); Loison et al. (2019) for  $C_4H_2$  are also smaller than the abundances we measured at the equator (by up to a factor 10) at 85 km. The nominal model of Vuitton et al. (2019) overestimates by a factor 10  $C_4H_2$  abundances, but their model without H heterogeneous loss (loss of hydrogen atoms when they interact with the surface of aerosols) is in very good agreement with our CIRS measurements. This is consistent with what Mathé et al. (2019) noted with their own CIRS observations at higher altitudes.

At high latitudes, we measure an enrichment in  $C_3H_4$  and  $C_4H_2$  compared to the equator (by a factor 17 for  $C_3H_4$  and 10 for  $C_4H_2$  at  $85^\circ S$  in November 2015 at 225 km). This is in good agreement with the results from previous studies (e.g Coustenis et al. 2019; Mathé et al. 2019; Teanby et al. 2019), especially if we take into account the strong dynamical activity and rapid evolution of the poles, for instance when the South Pole goes from autumn to winter solstice, as illustrated by the differences between the profiles measured at  $84^\circ S$  in September 2015 and January 2016 by Mathé et al. (2019) (see fig. 4), and as described by Teanby et al. (2017). This is due to the atmospheric circulation that evolves from 2 equator-to-poles cells at the equinox, to a single pole-to-pole cell with a strong subsidence above the autumn/winter pole that advects photochemical products from

their production area in the upper atmosphere to the lower atmosphere, as shown in Titan's **General Circulation Models** (GCM, Vatan d'Ollone et al., *in prep*, Vatan d'Ollone et al. 2017; Lebonnois et al. 2012; Lora et al. 2015; Newman et al. 2011). At high northern latitudes,  $C_3H_4$  and  $C_4H_2$  abundances have decreased slightly from March 2005 to July 2015 i.e. from winter to late spring. This confirms previous observations of Sylvestre et al. (2018) (at 85 km) and Mathé et al. (2019) (in the 175-280 km altitude range) where the enrichment in photochemical species at the North pole persists up to January 2015 in the lower stratosphere, whereas a depletion is observed in the upper stratosphere from December 2011 (Vinatier et al. 2015; Mathé et al. 2019). These observations are consistent with the persistence of a small circulation cell above the high northern latitudes during the transition from the two equator-to-poles cells to a single pole-to-pole during most of the northern spring as predicted by the LMDZ GCM (Vatan d'Ollone et al. 2017; Lebonnois et al. 2012) (see also figure 12 of Sylvestre et al. (2018)). In July 2015, this residual circulation cell has disappeared, thus allowing the depletion in trace gases of the lower stratosphere by upwelling.

### 3.2. $C_2N_2$

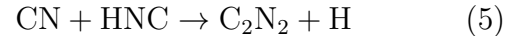
Panel (c) of fig. 4 shows the  $C_2N_2$  profiles we measured at different latitudes and seasons. At the equator, we measured an average profile over the Cassini mission where  $C_2N_2$  increases from  $5.0 \pm 1.5 \times 10^{-11}$  at 85 km to  $6.2 \pm 0.8 \times 10^{-11}$  at 125 km, and a  $3 - \sigma$  upper limit of  $2.5 \times 10^{-10}$  at 225 km. In the southern hemisphere in summer (2005-2009) we were able to measure an abundance of  $6.8 \pm 0.6 \times 10^{-10}$  for  $C_2N_2$  at 225 km. The  $C_2N_2$  abundances retrieved from **the southern summer dataset** below 225 km are smaller than the abundances at the equator, similar to what was measured

482 for  $C_4H_2$  and  $C_3H_4$ . The LMDZ GCM predicts  
 483 that during northern winter the upwelling due  
 484 to the ascending branch of the pole-to-pole cell  
 485 is the strongest above southern mid-latitudes.  
 486 Air depleted in photochemical products (due to  
 487 their condensation) is thus advected upward in  
 488 the southern hemisphere, which explains why  
 489 it has lower  $C_2N_2$ ,  $C_3H_4$ , and  $C_4H_2$  than at the  
 490 equator.

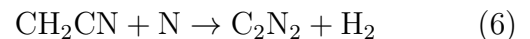
491  
 492 At high latitudes, our measurements are con-  
 493 sistent with the profile at  $70^\circ N$  by [Coustenis](#)  
 494 [et al. \(1991\)](#).  $C_2N_2$  profiles exhibit a strong en-  
 495 richment compared to our equatorial or south-  
 496 ern hemisphere summer averages. This trend is  
 497 similar to the measurements of  $C_2N_2$  at 15 mbar  
 498 (85 km) by [Sylvestre et al. \(2018\)](#), and to what  
 499 has been measured for  $C_3H_4$  and  $C_4H_2$ . The  
 500 seasonal evolution of  $C_2N_2$  at high northern  
 501 latitudes is also very similar to the evolution  
 502 of  $C_4H_2$  and  $C_3H_4$ , with a slight decrease from  
 503 northern winter (2005) to late spring (2015).  
 504 The enrichment in  $C_2N_2$  at the poles is much  
 505 larger than the enrichment in  $C_3H_4$  and  $C_4H_2$ .  
 506 For instance, in our results,  $85^\circ S$  in 2015, the  
 507  $C_2N_2$  volume mixing ratio at 225 km was at  
 508 least 100 times larger than at the equator,  
 509 whereas  $C_3H_4$  and  $C_4H_2$  abundances were re-  
 510 spectively 17 and 10 times larger than at the  
 511 equator. This is consistent with the results of  
 512 [Teanby et al. \(2010\)](#) where nitriles were more  
 513 enriched than hydrocarbons with similar pho-  
 514 tochemical lifetimes, which could indicate the  
 515 presence of an additional loss process for ni-  
 516 triles.

517  
 518 In fig. 4, the CIRS profiles of  $C_2N_2$  are com-  
 519 pared with the profiles predicted by the photo-  
 520 chemical models of [Vuitton et al. \(2019\)](#) (Model  
 521 V19 in fig. 4) and of [Dobrijevic et al. \(2016\)](#);  
 522 [Loison et al. \(2015\)](#) (Model D16 in fig. 4). The  
 523 abundances we measured at the equator and  
 524 in the southern hemisphere in summer are the

525 same order of magnitude as the predictions of  
 526 [Dobrijevic et al. \(2016\)](#) and 1-2 orders of mag-  
 527 nitude larger than the results of [Vuitton et al.](#)  
 528 [\(2019\)](#). This may be explained by the differ-  
 529 ent chemical reaction schemes of these two mod-  
 530 els, and more particularly in the main produc-  
 531 tion reactions for  $C_2N_2$ , which for [Vuitton et al.](#)  
 532 [\(2019\)](#) is:



533 and for [Dobrijevic et al. \(2016\)](#) is:



534 which is not taken into account into the model  
 535 of [Vuitton et al. \(2019\)](#). However, significant  
 536 uncertainties remain about the kinetics of re-  
 537 action 6 ([V. Vuitton, personal communication](#)).  
 538 In both models, the main loss reaction in the  
 539 lower stratosphere is:



540 unlike the photochemical model of [Krasnopol-](#)  
 541 [sky \(2014\)](#), where  $C_2N_2$  is mainly lost by pho-  
 542 todissociation and where the  $C_2N_2$  abundance  
 543 is overestimated by a factor 60.

544  
 545 Galactic Cosmic Rays (GCR) ionize  $N_2$  in  
 546 the lower stratosphere with a magnitude com-  
 547 parable to solar UV in the upper atmosphere  
 548 ([Gronoff et al. 2009](#)), hence creating a second  
 549 production region for  $C_2N_2$  at lower altitude  
 550 in photochemical models. In [Vuitton et al.](#)  
 551 [\(2019\)](#) and [Dobrijevic et al. \(2016\)](#), instead of  
 552 increasing with altitude like  $C_4H_2$  abundance,  
 553  $C_2N_2$  profile exhibits a local maximum between  
 554 100 km and 200 km (see fig. 4). Below 100 km,  
 555  $C_2N_2$  abundance decreases with decreasing al-  
 556 titude as this gas reacts with other species  
 557 and condenses. When we compare the profiles  
 558 of  $C_2N_2$  from [Dobrijevic et al. \(2016\)](#) with and  
 559 without GCR, our measurements at the equator  
 560 and in the southern hemisphere in summer are

561 in good agreement with the profile with GCR  
 562 at 225 km, but not in agreement with either  
 563 profiles below 125 km, where photochemical  
 564 models predict a local maximum of  $C_2N_2$  due  
 565 to the GCR. This seems to indicate a smaller  
 566 influence of the GCR on  $C_2N_2$  profile than pre-  
 567 dicted by the models. However, their effect can  
 568 not be completely ruled out as we do not ob-  
 569 serve the steep decrease with pressure predicted  
 570 without GCR.

571  
 572 Many other nitrogen-bearing species are pre-  
 573 dicted to be affected by the GCR bombardment.  
 574 For instance, in [Dobrijevic et al. \(2016\)](#), HNC  
 575 is predicted to be up to 100 times more abun-  
 576 dant below 600 km when effects of GCR bom-  
 577 bardment are included. However, recent ALMA  
 578 measurements of the vertical profile of HNC are  
 579 in better agreement with the predictions of [Do-  
 580 brijevic et al. \(2016\)](#) without the effects of GCR  
 581 ([Lellouch et al. 2019](#)). GCR may also have a  
 582 strong effect on the  $^{14}N/^{15}N$  ratios in  $C_2H_5CN$   
 583 and  $CH_3CN$ , as they could be up to twice as  
 584 high as in HCN or  $HC_3N$  ([Dobrijevic & Loison  
 585 2018](#)). [Iino et al. \(2020\)](#) ALMA measurements  
 586 of  $^{14}N/^{15}N$  in  $CH_3CN$  were not inconsistent with  
 587 these predictions, but not precise enough to be  
 588 conclusive. The production of amines (e.g  $NH_3$ ,  
 589  $CH_3NH_2$ ,  $CH_3NHCH_3$ ), imines (e.g  $CH_2NH$ ),  
 590 and aromatics could also be increased by the  
 591 GCR (by up to 3 orders of magnitude for amines  
 592 and imines, [Loison et al. 2015, 2019](#)), but obser-  
 593 vational data are insufficient for these species.

### 594 3.3. $H_2O$

595 Panel (d) of [fig. 4](#) presents our measurements  
 596 for the  $H_2O$  abundances. At the equator, the  
 597 abundance of water increases with altitude from  
 598  $1.6 \pm 0.1 \times 10^{-10}$  at 100 km to  $8.2 \pm_{1.2}^{1.8} \times 10^{-10}$   
 599 at 225 km. In the lower atmosphere, our results  
 600 are consistent with the Cassini/CIRS measure-  
 601 ments of [Cottini et al. \(2012\)](#) (see [fig. 4](#)) and  
 602 of [Bauduin et al. \(2018\)](#), and about one order  
 603 of magnitude larger than the Herschel mea-

604 surements of [Moreno et al. \(2012\)](#). [Bauduin  
 605 et al. \(2018\)](#) explained the inconsistency be-  
 606 tween the CIRS and Herschel results by po-  
 607 tential meridional and seasonal variations in  
 608  $H_2O$  abundance. At 225 km, we measured a  
 609  $H_2O$  abundance twice as large as [Cottini et al.  
 610 \(2012\)](#). In the southern hemisphere in summer,  
 611  $H_2O$  abundance is within error bars from the  
 612 equatorial measurements at all probed altitudes  
 613 unlike  $C_3H_4$ ,  $C_4H_2$  and  $C_2N_2$  for which volume  
 614 mixing ratios are significantly smaller in the  
 615 southern hemisphere than at the equator be-  
 616 low 125 km. This difference of behaviour is  
 617 expected as  $H_2O$  is predicted to have a much  
 618 longer lifetime than  $C_3H_4$ ,  $C_4H_2$ , and  $C_2N_2$ .  
 619 At the poles, we could only measure  $3 - \sigma$  up-  
 620 per limits of  $H_2O$  which allow us to say that  
 621 autumn/winter poles can not be enriched in  
 622 water by more than a factor 10 compared to  
 623 the equator at 225 km. These results are not  
 624 inconsistent with the meridional and seasonal  
 625 variations in water distribution suggested by  
 626 [Bauduin et al. \(2018\)](#) to explain the differences  
 627 between the Cassini/CIRS and the Herschel  
 628 results.

629  
 630 Our  $H_2O$  profiles are also compared to the  
 631 photochemical models of [Dobrijevic et al.  
 632 \(2016\)](#); [Loison et al. \(2019\)](#) (Model D16 in [fig.  
 633 4](#)) and [Vuitton et al. \(2019\)](#) (Model V19 in [fig.  
 634 4](#)). The profile from [Vuitton et al. \(2019\)](#) is in  
 635 good agreement with our measurements at the  
 636 equator and **in the southern hemisphere in  
 637 summer** whereas the predictions of [Dobrijevic  
 638 et al. \(2016\)](#); [Loison et al. \(2019\)](#) are one order  
 639 of magnitude smaller than our results. As [Do-  
 640 brijevic et al. \(2016\)](#) used the results of [Moreno  
 641 et al. \(2012\)](#) to constrain the eddy diffusion  
 642 coefficient in their model, the good agreement  
 643 between these two studies is expected. More  
 644 measurements of  $H_2O$  abundance are required  
 645 to constrain further its variations and under-  
 646 stand the processes that shape its vertical and

647 meridional distribution.

648

649

#### 4. CONCLUSION

650 In this paper, we present the first study of  
 651 the  $C_2N_2$  vertical distribution for different lati-  
 652 tudes and seasons in Titan’s stratosphere, using  
 653 Cassini/CIRS measurements. At the equator  
 654 we measured a  $C_2N_2$  abundance increasing with  
 655 altitude, from  $5.0 \pm 1.5 \times 10^{-11}$  at 85 km to  
 656  $6.2 \pm 0.8 \times 10^{-11}$  at 125 km and a  $3\text{-}\sigma$  upper  
 657 limit of  $2.5 \times 10^{-10}$  at 225 km. Poles are enriched  
 658 in  $C_2N_2$ , by up to a factor 100 compared to the  
 659 equator. Comparing these vertical profiles with  
 660 the predictions of recent photochemical models  
 661 helps to constrain the chemistry of this gas, es-  
 662 pecially on the role of the Galactic Cosmic Rays  
 663 that seem less important than predicted in the  
 664 models. These data also allowed us to measure  
 665 profiles of  $C_3H_4$  and  $C_4H_2$  in the lower part of  
 666 the stratosphere (down to 85 km), which is usu-  
 667 ally not probed by mid-infrared Cassini/CIRS  
 668 observations. We could thus extend the descrip-  
 669 tion of the meridional and seasonal variations

677

## APPENDIX

678

### A. ANALYSED DATASETS

**Table 1.** Cassini CIRS nadir datasets analysed in this study. N is the number of spectra measured during the acquisition. Asterisks denote the datasets used in the Equatorial Average. † denote the datasets used in the Southern Summer Hemisphere Average.

| Dataset                       | Date         | N   | Latitude (°N) |
|-------------------------------|--------------|-----|---------------|
| CIRS_000TLFIRNADCMP017_PRIME† | 3 Jul. 2004  | 13  | -35.5         |
| CIRS_003TLFIRNADCMP002_PRIME† | 15 Feb. 2005 | 180 | -18.7         |
| CIRS_005TLFIRNADCMP002_PRIME† | 31 Mar. 2005 | 241 | -41.1         |
| CIRS_00BTLFIRNADCMP001_PRIME  | 12 Dec. 2004 | 224 | 16.4          |
| CIRS_013TLFIRNADCMP004_PRIME† | 22 Aug. 2005 | 248 | -53.7         |

**Table 1** *continued*

670 of these species to this part of Titan’s atmo-  
 671 sphere. This study also provides insights on  
 672 the variations of the  $H_2O$  abundance in Titan’s  
 673 lower atmosphere, including upper limits on its  
 674 potential enrichment by the atmospheric circu-  
 675 lation at the poles (up to a factor 10).

676

### ACKNOWLEDGMENTS

This research was funded by the UK Sci-  
 ences and Technology Facilities Research coun-  
 cil (grant number ST/R000980/1) and the  
 Cassini project. This research made use of  
 Astropy, a community-developed core Python  
 package for Astronomy ([Astropy Collaboration  
 et al. 2013](#)), and matplotlib, a Python library  
 for publication quality graphics ([Hunter 2007](#)).  
 We thank Jan Vatant d’Ollone for insightful  
 discussions about the predictions of the LMDZ  
 GCM, Véronique Vuitton for useful comments  
 about Titan’s photochemistry, and the anony-  
 mous reviewer for their suggestions.

**Table 1** (*continued*)

| Dataset                         | Date         | N   | Latitude (°N) |
|---------------------------------|--------------|-----|---------------|
| CIRS_019TI.FIRNADCMP002_PRIME†  | 26 Dec. 2005 | 124 | -0.0          |
| CIRS_021TI.FIRNADCMP002_PRIME†  | 27 Feb. 2006 | 213 | -30.2         |
| CIRS_022TI.FIRNADCMP003_PRIME†* | 18 Mar. 2006 | 401 | -0.4          |
| CIRS_023TI.FIRNADCMP002_PRIME†  | 1 May 2006   | 215 | -35.0         |
| CIRS_024TI.FIRNADCMP003_PRIME†* | 19 May 2006  | 350 | -15.5         |
| CIRS_029TI.FIRNADCMP003_PRIME*  | 23 Sep. 2006 | 312 | 9.5           |
| CIRS_030TI.FIRNADCMP002_PRIME†  | 10 Oct. 2006 | 340 | -59.1         |
| CIRS_035TI.FIRNADCMP023_PRIME†  | 12 Dec. 2006 | 164 | -73.3         |
| CIRS_036TI.FIRNADCMP002_PRIME†  | 28 Dec. 2006 | 136 | -89.1         |
| CIRS_037TI.FIRNADCMP002_PRIME†  | 13 Jan. 2007 | 107 | -70.3         |
| CIRS_038TI.FIRNADCMP002_PRIME†  | 29 Jan. 2007 | 254 | -39.7         |
| CIRS_040TI.FIRNADCMP001_PRIME†  | 09 Mar. 2007 | 159 | -49.2         |
| CIRS_041TI.FIRNADCMP001_PRIME†  | 25 Mar. 2007 | 2   | -76.8         |
| CIRS_042TI.FIRNADCMP001_PRIME†  | 10 Apr 2007  | 103 | -60.8         |
| CIRS_043TI.FIRNADCMP001_PRIME†  | 26 Apr 2007  | 263 | -51.4         |
| CIRS_044TI.FIRNADCMP002_PRIME*† | 13 May 2007  | 104 | -0.5          |
| CIRS_045TI.FIRNADCMP001_PRIME†  | 28 May 2007  | 231 | -22.3         |
| CIRS_046TI.FIRNADCMP001_PRIME*  | 13 Jun. 2007 | 60  | 17.6          |
| CIRS_046TI.FIRNADCMP002_PRIME†  | 14 Jun. 2007 | 102 | -20.8         |
| CIRS_047TI.FIRNADCMP001_PRIME*  | 29 Jun. 2007 | 204 | 9.8           |
| CIRS_048TI.FIRNADCMP001_PRIME†  | 18 Jul. 2007 | 96  | -34.8         |
| CIRS_050TI.FIRNADCMP001_PRIME†* | 1 Oct. 2007  | 144 | -10.1         |
| CIRS_053TI.FIRNADCMP001_PRIME†  | 04 Dec. 2007 | 223 | -40.2         |
| CIRS_055TI.FIRNADCMP001_PRIME*  | 05 Jan. 2008 | 190 | 18.7          |
| CIRS_059TI.FIRNADCMP001_PRIME†  | 22 Feb. 2008 | 172 | -24.9         |
| CIRS_059TI.FIRNADCMP002_PRIME*  | 23 Feb. 2008 | 98  | 17.1          |
| CIRS_067TI.FIRNADCMP001_PRIME†  | 11 May 2008  | 48  | -59.5         |
| CIRS_069TI.FIRNADCMP001_PRIME†  | 27 May 2008  | 112 | -44.6         |
| CIRS_069TI.FIRNADCMP002_PRIME*  | 28 May 2008  | 112 | 9.5           |
| CIRS_095TI.FIRNADCMP001_PRIME†* | 05 Dec. 2008 | 213 | -14.0         |
| CIRS_097TI.FIRNADCMP001_PRIME†* | 20 Dec. 2008 | 231 | -10.9         |
| CIRS_106TI.FIRNADCMP001_PRIME†  | 26 Mar. 2009 | 165 | -60.3         |
| CIRS_110TI.FIRNADCMP001_PRIME†  | 06 May 2009  | 282 | -68.1         |
| CIRS_111TI.FIRNADCMP002_PRIME†  | 22 May 2009  | 168 | -27.1         |

**Table 1** *continued*



**Table 1** (*continued*)

| Dataset                        | Date         | N   | Latitude (°N) |
|--------------------------------|--------------|-----|---------------|
| CIRS_112TI.FIRNADCMP002_PRIME† | 7 Jun. 2009  | 274 | -58.9         |
| CIRS_114TI.FIRNADCMP001_PRIME† | 9 Jul. 2009  | 164 | -71.4         |
| CIRS_119TI.FIRNADCMP001_PRIME† | 11 Oct. 2009 | 5   | -25.9         |
| CIRS_119TI.FIRNADCMP002_PRIME* | 12 Oct. 2009 | 166 | 0.4           |
| CIRS_123TI.FIRNADCMP002_PRIME† | 28 Dec. 2009 | 186 | -46.1         |
| CIRS_124TI.FIRNADCMP002_PRIME* | 13 Jan. 2010 | 272 | -1.2          |
| CIRS_131TI.FIRNADCMP002_PRIME* | 20 May 2010  | 229 | -19.8         |
| CIRS_133TI.FIRNADCMP001_PRIME* | 20 Jun. 2010 | 187 | -49.7         |
| CIRS_134TI.FIRNADCMP001_PRIME* | 06 Jul. 2010 | 251 | -10.0         |
| CIRS_138TI.FIRNADCMP001_PRIME* | 24 Sep. 2010 | 190 | -30.1         |
| CIRS_148TI.FIRNADCMP001_PRIME* | 8 May 2011   | 200 | -10.0         |
| CIRS_153TI.FIRNADCMP001_PRIME* | 11 Sep. 2011 | 227 | 9.9           |
| CIRS_160TI.FIRNADCMP002_PRIME* | 30 Jan. 2012 | 280 | -0.2          |
| CIRS_161TI.FIRNADCMP001_PRIME* | 18 Feb. 2012 | 121 | 9.9           |
| CIRS_161TI.FIRNADCMP002_PRIME* | 19 Feb. 2012 | 89  | -15.0         |
| CIRS_166TI.FIRNADCMP001_PRIME* | 22 May 2012  | 318 | -19.9         |
| CIRS_169TI.FIRNADCMP001_PRIME* | 24 Jul. 2012 | 258 | -9.7          |
| CIRS_175TI.FIRNADCMP001_PRIME* | 28 Nov. 2012 | 150 | 15.0          |
| CIRS_185TI.FIRNADCMP001_PRIME* | 05 Apr 2013  | 244 | 15.0          |
| CIRS_190TI.FIRNADCMP001_PRIME* | 23 May 2013  | 224 | -0.2          |
| CIRS_195TI.FIRNADCMP001_PRIME* | 25 Jul. 2013 | 186 | 19.6          |
| CIRS_201TI.FIRNADCMP001_PRIME* | 02 Feb. 2014 | 329 | 19.9          |
| CIRS_203TI.FIRNADCMP002_PRIME* | 07 Apr 2014  | 239 | 0.5           |
| CIRS_207TI.FIRNADCMP002_PRIME  | 21 Aug. 2014 | 163 | 79.7          |
| CIRS_248TI.FIRNADCMP001_PRIME  | 13 Nov. 2016 | 185 | -88.9         |

## REFERENCES

- 679 Astropy Collaboration, Robitaille, T. P., Tollerud,  
680 E. J., et al. 2013, *A&A*, 558, A33,  
681 doi: [10.1051/0004-6361/201322068](https://doi.org/10.1051/0004-6361/201322068)
- 682 Bauduin, S., Irwin, P. G. J., Lellouch, E., et al.  
683 2018, *Icarus*, 311, 288,  
684 doi: [10.1016/j.icarus.2018.04.003](https://doi.org/10.1016/j.icarus.2018.04.003)
- 685 Bézard, B. 2014, *Icarus*, 242, 64,  
686 doi: [10.1016/j.icarus.2014.07.013](https://doi.org/10.1016/j.icarus.2014.07.013)
- 687 Borysow, A., & Frommhold, L. 1986a, *ApJ*, 311,  
688 1043, doi: [10.1086/164841](https://doi.org/10.1086/164841)
- 689 —. 1986b, *ApJ*, 303, 495, doi: [10.1086/164096](https://doi.org/10.1086/164096)
- 690 —. 1987, *ApJ*, 318, 940, doi: [10.1086/165426](https://doi.org/10.1086/165426)
- 691 Borysow, A., & Tang, C. 1993, *Icarus*, 105, 175,  
692 doi: [10.1006/icar.1993.1117](https://doi.org/10.1006/icar.1993.1117)
- 693 Bézard, B., & Vinatier, S. 2019, *Icarus*, doi: <https://doi.org/10.1016/j.icarus.2019.03.038>
- 694

**Table 2.** Cassini CIRS limb datasets analysed in this study. N is the number of spectra measured during the acquisition. Asterisks denote the datasets used in the Equatorial Average. † denote the datasets used in the Southern Hemisphere Summer Average.

| Dataset                         | Date         | N  | Latitude (°N) |
|---------------------------------|--------------|----|---------------|
| CIRS_005TI_FIRLMBINT002_PRIME   | 31 Mar. 2005 | 26 | 84.6          |
| CIRS_013TI_FIRLMBINT002_PRIME†  | 22 Aug. 2005 | 58 | -54.5         |
| CIRS_013TI_FIRLMBINT003_PRIME†  | 22 Aug. 2005 | 58 | -54.5         |
| CIRS_028TI_FIRLMBINT002_PRIME*† | 7 Sep. 2006  | 54 | -15.3         |
| CIRS_029TI_FIRLMBINT003_PRIME*  | 23 Sep. 2006 | 70 | 30.0          |
| CIRS_038TI_FIRLMBINT001_PRIME*  | 29 Jan. 2007 | 26 | 28.7          |
| CIRS_040TI_FIRLMBINT001_PRIME*  | 9 Mar. 2007  | 35 | 9.6           |
| CIRS_040TI_FIRLMBINT002_PRIME*  | 10 Mar. 2007 | 29 | 14.8          |
| CIRS_052TI_FIRLMBINT001_PRIME†  | 18 Nov. 2007 | 24 | -79.9         |
| CIRS_053TI_FIRLMBINT001_PRIME*† | 4 Dec. 2007  | 79 | 0.2           |
| CIRS_055TI_FIRLMBINT001_PRIME*† | 5 Jan. 2008  | 54 | -29.9         |
| CIRS_062TI_FIRLMBINT003_PRIME†  | 25 Mar. 2008 | 49 | -55.3         |
| CIRS_093TI_FIRLMBINT002_PRIME†  | 19 Nov. 2008 | 74 | -44.9         |
| CIRS_095TI_FIRLMBINT001_PRIME†  | 5 Dec. 2008  | 54 | -35.1         |
| CIRS_095TI_FIRLMBINT002_PRIME*† | 5 Dec. 2008  | 76 | -25.0         |
| CIRS_097TI_FIRLMBINT001_PRIME*  | 21 Dec. 2008 | 55 | 10.1          |
| CIRS_110TI_FIRLMBINT001_PRIME*  | 5 May 2009   | 51 | 20.1          |
| CIRS_113TI_FIRLMBINT001_PRIME*† | 22 Jun. 2009 | 59 | -10.0         |
| CIRS_115TI_FIRLMBINT002_PRIME†  | 24 Jul. 2009 | 51 | -60.0         |
| CIRS_119TI_FIRLMBINT002_PRIME†  | 12 Oct. 2009 | 60 | -75.0         |
| CIRS_125TI_FIRLMBINT001_PRIME*  | 28 Jan. 2010 | 68 | 29.9          |
| CIRS_175TI_FIRLMBINT001_PRIME*  | 29 Nov. 2012 | 70 | -2.0          |
| CIRS_185TI_FIRLMBINT001_PRIME*  | 5 Apr. 2013  | 70 | 14.0          |
| CIRS_200TI_FIRLMBINT002_PRIME*  | 1 Jan. 2014  | 49 | -24.0         |
| CIRS_206TI_FIRLMBINT005_PRIME*  | 20 Jul. 2014 | 65 | 3.5           |
| CIRS_208TI_FIRLMBINT002_PRIME*  | 22 Sep. 2014 | 70 | 28.1          |
| CIRS_218TI_FIRLMBINT001_PRIME   | 7 Jul. 2015  | 51 | 80.1          |
| CIRS_225TI_FIRLMBINT002_PRIME   | 13 Nov. 2015 | 53 | -84.6         |

695 Cottini, V., Nixon, C. A., Jennings, D. E., et al.  
696 2012, *Icarus*, 220, 855,  
697 doi: [10.1016/j.icarus.2012.06.014](https://doi.org/10.1016/j.icarus.2012.06.014)

698 Coustenis, A., & Bezaud, B. 1995, *Icarus*, 115,  
699 126, doi: [10.1006/icar.1995.1084](https://doi.org/10.1006/icar.1995.1084)

700 Coustenis, A., Bezaud, B., Gautier, D., Marten,  
701 A., & Samuelson, R. 1991, *Icarus*, 89, 152,  
702 doi: [10.1016/0019-1035\(91\)90095-B](https://doi.org/10.1016/0019-1035(91)90095-B)

703 Coustenis, A., Jennings, D., Achterberg, R., et al.  
704 2019, *Icarus*, 113413, doi: <https://doi.org/10.1016/j.icarus.2019.113413>  
705

- 706 Coustenis, A., Salama, A., Lellouch, E., et al.  
707 1998, *A&A*, 336, L85
- 708 Cui, J., Yelle, R. V., Vuitton, V., et al. 2009,  
709 *Icarus*, 200, 581,  
710 doi: [10.1016/j.icarus.2008.12.005](https://doi.org/10.1016/j.icarus.2008.12.005)
- 711 de Kok, R., Irwin, P. G. J., Teanby, N. A., et al.  
712 2007, *Icarus*, 191, 223,  
713 doi: [10.1016/j.icarus.2007.04.003](https://doi.org/10.1016/j.icarus.2007.04.003)
- 714 —. 2010, *Icarus*, 207, 485,  
715 doi: [10.1016/j.icarus.2009.10.021](https://doi.org/10.1016/j.icarus.2009.10.021)
- 716 Dobrijevic, M., Hébrard, E., Loison, J. C., &  
717 Hickson, K. M. 2014, *Icarus*, 228, 324,  
718 doi: [10.1016/j.icarus.2013.10.015](https://doi.org/10.1016/j.icarus.2013.10.015)
- 719 Dobrijevic, M., & Loison, J. C. 2018, *Icarus*, 307,  
720 371, doi: [10.1016/j.icarus.2017.10.027](https://doi.org/10.1016/j.icarus.2017.10.027)
- 721 Dobrijevic, M., Loison, J. C., Hickson, K. M., &  
722 Gronoff, G. 2016, *Icarus*, 268, 313,  
723 doi: [10.1016/j.icarus.2015.12.045](https://doi.org/10.1016/j.icarus.2015.12.045)
- 724 Flasar, F. M., Kunde, V. G., Abbas, M. M., et al.  
725 2004, *SSRv*, 115, 169,  
726 doi: [10.1007/s11214-004-1454-9](https://doi.org/10.1007/s11214-004-1454-9)
- 727 Gronoff, G., Lilensten, J., Desorgher, L., &  
728 Flückiger, E. 2009, *A&A*, 506, 955,  
729 doi: [10.1051/0004-6361/200912371](https://doi.org/10.1051/0004-6361/200912371)
- 730 Hörst, S. M., Vuitton, V., & Yelle, R. V. 2008,  
731 *Journal of Geophysical Research (Planets)*, 113,  
732 E10006, doi: [10.1029/2008JE003135](https://doi.org/10.1029/2008JE003135)
- 733 Hunter, J. D. 2007, *Computing in Science &*  
734 *Engineering*, 9, 90, doi: [10.1109/MCSE.2007.55](https://doi.org/10.1109/MCSE.2007.55)
- 735 Iino, T., Sagawa, H., & Tsukagoshi, T. 2020, *ApJ*,  
736 890, 95, doi: [10.3847/1538-4357/ab66b0](https://doi.org/10.3847/1538-4357/ab66b0)
- 737 Irwin, P. G. J., Teanby, N. A., de Kok, R., et al.  
738 2008, *JQSRT*, 109, 1136,  
739 doi: [10.1016/j.jqsrt.2007.11.006](https://doi.org/10.1016/j.jqsrt.2007.11.006)
- 740 Jennings, D. E., Flasar, F. M., Kunde, V. G.,  
741 et al. 2017, *ApOpt*, 56, 5274,  
742 doi: [10.1364/ao.56.005274](https://doi.org/10.1364/ao.56.005274)
- 743 Krasnopolsky, V. A. 2014, *Icarus*, 236, 83,  
744 doi: [10.1016/j.icarus.2014.03.041](https://doi.org/10.1016/j.icarus.2014.03.041)
- 745 Lebonnois, S., Burgalat, J., Rannou, P., &  
746 Charnay, B. 2012, *Icarus*, 218, 707,  
747 doi: [10.1016/j.icarus.2011.11.032](https://doi.org/10.1016/j.icarus.2011.11.032)
- 748 Lellouch, E., Bézard, B., Flasar, F. M., et al.  
749 2014, *Icarus*, 231, 323,  
750 doi: [10.1016/j.icarus.2013.12.016](https://doi.org/10.1016/j.icarus.2013.12.016)
- 751 Lellouch, E., Gurwell, M. A., Moreno, R., et al.  
752 2019, *Nature Astronomy*, 3, 614,  
753 doi: [10.1038/s41550-019-0749-4](https://doi.org/10.1038/s41550-019-0749-4)
- 754 Loison, J. C., Dobrijevic, M., & Hickson, K. M.  
755 2019, *Icarus*, 329, 55,  
756 doi: [10.1016/j.icarus.2019.03.024](https://doi.org/10.1016/j.icarus.2019.03.024)
- 757 Loison, J. C., Hébrard, E., Dobrijevic, M., et al.  
758 2015, *Icarus*, 247, 218,  
759 doi: [10.1016/j.icarus.2014.09.039](https://doi.org/10.1016/j.icarus.2014.09.039)
- 760 Lombardo, N. A., Nixon, C. A., Achterberg,  
761 R. K., et al. 2019a, *Icarus*, 317, 454,  
762 doi: [10.1016/j.icarus.2018.08.027](https://doi.org/10.1016/j.icarus.2018.08.027)
- 763 Lombardo, N. A., Nixon, C. A., Sylvestre, M.,  
764 et al. 2019b, *AJ*, 157, 160,  
765 doi: [10.3847/1538-3881/ab0e07](https://doi.org/10.3847/1538-3881/ab0e07)
- 766 Lora, J. M., Lunine, J. I., & Russell, J. L. 2015,  
767 *Icarus*, 250, 516,  
768 doi: [10.1016/j.icarus.2014.12.030](https://doi.org/10.1016/j.icarus.2014.12.030)
- 769 Lutz, B. L., de Bergh, C., & Owen, T. 1983,  
770 *Science*, 220, 1374,  
771 doi: [10.1126/science.220.4604.1374](https://doi.org/10.1126/science.220.4604.1374)
- 772 Mathé, C., Vinatier, S., Bézard, B., et al. 2019,  
773 *Icarus*, 113547, doi: <https://doi.org/10.1016/j.icarus.2019.113547>
- 774 Moreno, R., Lellouch, E., Lara, L. M., et al. 2012,  
775 *Icarus*, 221, 753,  
776 doi: [10.1016/j.icarus.2012.09.006](https://doi.org/10.1016/j.icarus.2012.09.006)
- 777 Newman, C. E., Lee, C., Lian, Y., Richardson,  
778 M. I., & Toigo, A. D. 2011, *Icarus*, 213, 636,  
779 doi: [10.1016/j.icarus.2011.03.025](https://doi.org/10.1016/j.icarus.2011.03.025)
- 780 Niemann, H. B., Atreya, S. K., Demick, J. E.,  
781 et al. 2010, *Journal of Geophysical Research*  
782 *(Planets)*, 115, E12006,  
783 doi: [10.1029/2010JE003659](https://doi.org/10.1029/2010JE003659)
- 784 Nixon, C. A., Ansty, T. M., Lombardo, N. A.,  
785 et al. 2019, *ApJS*, 244, 14,  
786 doi: [10.3847/1538-4365/ab3799](https://doi.org/10.3847/1538-4365/ab3799)
- 787 Samuelson, R. E., Maguire, W. C., Hanel, R. A.,  
788 et al. 1983, *J. Geophys. Res.*, 88, 8709,  
789 doi: [10.1029/JA088iA11p08709](https://doi.org/10.1029/JA088iA11p08709)
- 790 Sylvestre, M., Teanby, N., d'Ollone, J. V., et al.  
791 2019, *Icarus*, doi: <https://doi.org/10.1016/j.icarus.2019.02.003>
- 792 Sylvestre, M., Teanby, N. A., Vinatier, S.,  
793 Lebonnois, S., & Irwin, P. G. J. 2018, *A&A*,  
794 609, A64, doi: [10.1051/0004-6361/201630255](https://doi.org/10.1051/0004-6361/201630255)
- 795 Teanby, N. A., & Irwin, P. G. J. 2007, *Ap&SS*,  
796 310, 293, doi: [10.1007/s10509-007-9519-3](https://doi.org/10.1007/s10509-007-9519-3)
- 797 Teanby, N. A., Irwin, P. G. J., de Kok, R., et al.  
798 2009, *Icarus*, 202, 620,  
799 doi: [10.1016/j.icarus.2009.03.022](https://doi.org/10.1016/j.icarus.2009.03.022)
- 800  
801

- 802 Teanby, N. A., Irwin, P. G. J., de Kok, R., &  
803 Nixon, C. A. 2010, *Faraday Discussions*, 147,  
804 51, doi: [10.1039/c001690j](https://doi.org/10.1039/c001690j)
- 805 Teanby, N. A., Sylvestre, M., Sharkey, J., et al.  
806 2019, *Geophys. Res. Lett.*, 46, 3079,  
807 doi: [10.1029/2018GL081401](https://doi.org/10.1029/2018GL081401)
- 808 Teanby, N. A., Bézard, B., Vinatier, S., et al.  
809 2017, *Nature Communications*, 8, 1586,  
810 doi: [10.1038/s41467-017-01839-z](https://doi.org/10.1038/s41467-017-01839-z)
- 811 Vatant d'Ollone, J., Lebonnois, S., & Guerlet, S.  
812 2017, in *EGU General Assembly Conference*  
813 *Abstracts*, Vol. 19, 10169
- 814 Vinatier, S., Rannou, P., Anderson, C. M., et al.  
815 2012, *Icarus*, 219, 5,  
816 doi: [10.1016/j.icarus.2012.02.009](https://doi.org/10.1016/j.icarus.2012.02.009)
- 817 Vinatier, S., Bézard, B., Lebonnois, S., et al. 2015,  
818 *Icarus*, 250, 95, doi: [10.1016/j.icarus.2014.11.019](https://doi.org/10.1016/j.icarus.2014.11.019)
- 819 Vuitton, V., Yelle, R. V., Klippenstein, S. J.,  
820 Hörst, S. M., & Lavvas, P. 2019, *Icarus*, 324,  
821 120, doi: [10.1016/j.icarus.2018.06.013](https://doi.org/10.1016/j.icarus.2018.06.013)